

RESEARCH ARTICLE

A Nearly Optimal Chattering Reduction Method of Sliding Mode Control With an Application to a Two-wheeled Mobile Robot

Lei Guo* | Han Zhao | Yuan Song

¹School of Artificial Intelligence, Beijing University of Posts and Telecommunications, P.O. Box 108, No.10 Xi Tucheng Road, Haidian, Beijing, China

Correspondence

*Lei Guo, Beijing University of Posts and Telecommunications. Email: guolei@bupt.edu.cn

Abstract

The problem we focus on in this paper is to find a nearly optimal sliding mode controller of continuous-time nonlinear multiple-input multiple-output (MIMO) systems that can both reduce chattering and minimize the cost function, which is a measure of the performance index of dynamics systems. First, the deficiency of chattering in traditional SMC and the quasi-SMC method are analyzed in this paper. In quasi-SMC, the signum function of the traditional SMC is replaced with a continuous saturation function. Then, a chattering reduction algorithm based on integral reinforcement learning (IRL) is proposed. Under an initial sliding mode controller, the proposed method can learn the nearly optimal saturation function using policy iteration. To satisfy the requirement of the learned saturation function, we treat the problem of training the saturation function as the constraint of an optimization problem. The online neural network implementation of the proposed algorithm is presented based on symmetric radius basis functions and a regularized batch least-squares (BLS) algorithm to train the control law in this paper. Finally, two examples are simulated to verify the effectiveness of the proposed method. The second example is an application to a real-world dynamics model—a two-wheeled variable structure robot.

KEYWORDS:

Sliding mode control, chattering reduction, saturation function, integral reinforcement learning, neural networks.

1 | INTRODUCTION

Sliding mode control (SMC), also known as variable structure control, is one of the most classic feedback control algorithms. Unlike most control schemes, SMC has an infinite switching gain when the sliding mode variable approaches zero. Therefore, the controller can be robust to small disturbances when the state variable is close to the switching line (or manifold, more generally) $S = 0$. However, the state variable will periodically shuttle between two sides of the surface with high frequency and can never be strictly stabilized due to time-delays, model uncertainties and other factors of the controllers and sensors, which is also known as chattering¹.

The chattering phenomenon could be very harmful in the real-world applications, as illustrated by the example of a two-wheeled mobile robot designed in this paper. Similar to the inverted pendulum, the two-wheeled mobile robot has static instability and dynamics stability, and the corresponding controller needs to adjust the posture of the robot in real time. Owing to the

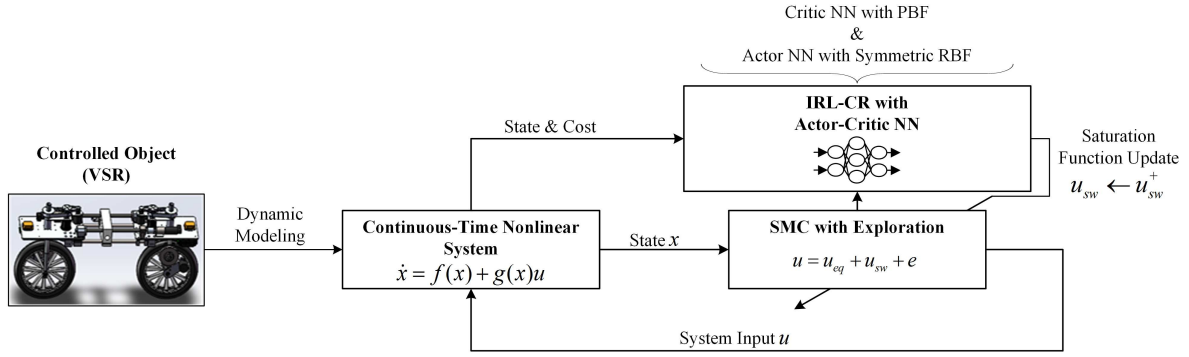


FIGURE 1 The control scheme of the method proposed in this paper.

mechanical transmission clearance, a high-frequency input signal cannot be perfectly executed by the actuator and can even damage it. Thus, the chattering needs to be reduced when SMC is applied to the robot controller.

The chattering reduction problem has been widely studied. The reaching control law was presented to reduce the amplitude of chattering and maintain a fast approach speed to the switching manifold². A method that can dynamically adjust the parameters of reaching law using fuzzy control was proposed in³. In these methods, the signum function still exists in the reaching law. Thus, the chattering cannot be completely eliminated.

Several methods based on high-order terminal SMC have also been proposed^{4,5,6}. However, the complexity of solving the control law and designing the switching manifolds limits their application to a real-world model. The quasi-sliding mode method is the most commonly used controller for reducing chattering. The main concept of quasi-SMC is to eliminate the discontinuous quantity of the signum function by replacing it with a continuous saturation function. A simple but effective way is to choose the piecewise linear (PWL) function as the saturation function⁷ and to make the switching gain a linear function of the sliding mode S in a boundary layer. The method of changing the boundary layer is presented in⁸. Similarly, other forms of saturation functions have been studied, e.g. hyperbolic tangent functions⁹. These functions are effective in avoiding the chattering phenomenon but were designed considering only the stability analysis, with the parameters set by experience and intuition. Little research has been focused on constructing and evaluating a standard performance index of quasi-sliding mode controllers.

The design of a saturation function such that the controller can simultaneously eliminate chattering and minimize the performance index is worth studying. In the following sections, it is considered a constrained optimization problem. Traditional optimal control methods, e.g., dynamic programming (DP)¹⁰, can theoretically solve the problem above. However, the DP algorithm must solve the Hamilton-Jacobi-Bellman (HJB) equation (or Bellman equation in a discrete-time system), which makes it difficult or even impossible to find the analytic solution when the model of a dynamics system is highly nonlinear, the state space has a high dimension, or the dynamics model is not precisely known.

Reinforcement learning (RL) is inspired by behavioral psychology and is a class of characteristic, data-driven algorithms used to learn a nearly optimal policy by interacting with the environment¹¹. RL is also called adaptive dynamics programming or approximate dynamic programming (ADP)¹² in the intelligent control field. In recent years, many RL algorithms have been combined with deep learning by using deep neural networks as function approximators. Many deep RL methods have been proposed^{13,14} and have efficient performances in different decision-making tasks^{15,16}. Unlike model-based controllers such as SMCs and optimal controllers, model-free deep RL methods do not require any *a priori* knowledge of the system dynamics. These algorithms, however, have not been proved to be convergent for continuous-time systems in the real-world¹⁷.

To ensure that our controller of continuous-time (CT) systems is admissible and able to converge during the learning phase, the controller design proposed in this paper is based on a class of ADP algorithms called integral reinforcement learning (IRL) algorithms¹⁸, which are used for solving the adaptive optimal control problem in CT dynamics systems, and its goal is to automatically learn an optimized saturation function from online data, which can both improve the performance index and simulate some features of the signum function nicely.

The rest of the paper is organized as follows. In Section 2, we discuss the mathematical form of sliding mode controllers and a chattering reduction versus performance optimization dilemma. Finding a suitable saturation function is considered an optimization problem in this section, and we introduce some features of the signum function as several constraint conditions. IRL algorithms are also mentioned as related works in this section. The design of a chattering reduction controller based on an

IRL algorithm, called integral Q-learning I¹⁹, is presented in Section 3. The learning algorithm proposed in this section should be used with a stabilized initial sliding mode controller to avoid massive inefficient exploratory actions and ensure convergence of the iterations. An online implementation of the algorithm using neural networks is also formulated in this paper. By adding a penalty term to the objective function and using a radius basis function neural network (RBFNN) to perform policy iteration, we transform the original problem into an unconstrained one. Section 4 gives two examples to verify the effectiveness of this method. The second example is a practical engineering application, that is, learning the controller of a variable structure wheeled robot working in the inverse pendulum (Segway) mode. Finally, conclusions are drawn in Section 5. The control scheme of the method proposed in this paper is shown in **FIGURE 1**.

As for notations, we use $\|x\|$ to denote the Euclidean norm $\sqrt{x^T x}$ of vector x . $X \otimes Y$ indicates the Kronecker product of the matrices X and Y throughout this paper. The function of time $x(t)$ is denoted as x_t or x , and the function of other variables $f(x)$ will be written as f in some equations for convenience.

2 | PROBLEM FORMULATION

2.1 | Sliding Mode Control with Boundary Layers

Consider the following continuous time system:

$$\dot{x}(t) = f(x(t)) + g(x(t))u(t), \quad (1)$$

where $x \in \mathbb{R}^n$ is the state variable and $u \in \mathbb{R}^m$ is the control input. It is assumed that system (1) can be stabilized on the set $\mathcal{D} \subseteq \mathbb{R}^n$ containing the origin and that $f : \mathcal{D} \rightarrow \mathbb{R}^n$ with $f(0) = 0$ and $g : \mathcal{D} \rightarrow \mathbb{R}^{n \times m}$ are Lipschitz on \mathcal{D} .

In conventional SMC, the switching manifolds are designed as straight lines. Thus, the sliding mode function is

$$S = C^T x = [s_1, s_2, \dots, s_m]^T, \quad (2)$$

where $C \in \mathbb{R}^{n \times m}$ is a constant matrix. Each element denotes a straight line $s_i = 0$ in the state space:

$$s_i = c_i^T x. \quad (3)$$

The sliding mode S indicates the expected motion law of the state values. The state of the dynamics system reach the switching manifold and move towards equilibrium.

Under the ideal condition, i.e., the state values stay on the manifold $S = 0$, the controller will ensure that the trajectories of x do not escape from the sliding surface. By solving the equation $\dot{S} = 0$, we can obtain the equivalent control law u_{eq} , which is also the general control law when $S = 0$, if $(C^T g)$ is a nonsingular matrix:

$$\begin{aligned} \dot{S} &= C^T \dot{x} \\ &= C^T (f(x) + g(x)u) = 0 \\ &\Rightarrow u_{eq} = -(C^T g)^{-1} C^T f. \end{aligned} \quad (4)$$

A few forms of the reaching control law that can switch the state to the sliding mode $S = 0$ has given in²⁰. Let $\dot{S} = -(W S + K \text{sgn}(S))$, where $W = \text{diag}(w_i)$, $K = \text{diag}(k_i) > 0$ ($i = 1, 2, \dots, m$); the switching control law can be obtained as

$$\begin{aligned} \dot{S} &= C^T (f(x) + g(x)u) = -(W S + K \text{sgn}(S)) \\ &\Rightarrow u_{sw} = -(C^T g)^{-1} (W S + K \text{sgn}(S)), \end{aligned} \quad (5)$$

where $\text{sgn}(S) = [\text{sgn}(s_1), \text{sgn}(s_2), \dots, \text{sgn}(s_m)]^T$ is the signum function, denoted as

$$\text{sgn}(s) = \begin{cases} -1 & s < 0 \\ 0 & s = 0, \\ 1 & s > 0 \end{cases} \quad (6)$$

and (5) is called the exponential velocity trending law.

The general control law is the sum of the two control laws above:

$$u = u_{eq} + u_{sw} = -(C^T g)^{-1} (C^T f + W S + K \text{sgn}(S)). \quad (7)$$

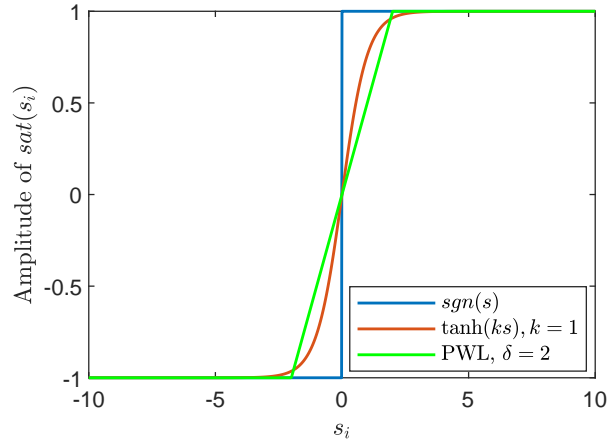


FIGURE 2 An example of different saturation functions: $sgn(s_i)$, $\tanh(ks_i)$ with $k = 1$ and the PWL function with $\delta = 2$.

Take the Lyapunov function as $V = \frac{1}{2}S^T S$ to analyze the stability of the system. The derivative of V with respect to time is

$$\dot{V} = S^T \dot{S} = -W S^T S - K \sum_{i=1}^m |s_i| < 0. \quad (8)$$

Thus, the state variable can converge to the equilibrium point.

The chattering phenomenon is mainly caused by the discontinuity of the signum function. An easy and effective way to solve this problem is to replace $sgn(S)$ with a continuous saturation function:

$$sat(S) = [sat(s_1), sat(s_2), \dots, sat(s_m)]^T. \quad (9)$$

The stability requirement (8) can be satisfied if $sat(s_i)$ meets the following conditions ($i = 1, 2, \dots, m$):

- (a) $sat(s_i) \cdot sgn(s_i) > 0$ ($s_i \neq 0$),
- (b) $sat(0) = 0$.

Three more conditions are proposed to simulate the signum function:

- (c) $\lim_{s_i \rightarrow \infty} sat(s_i) = sgn(s_i)$.
- (d) $sat(s_i)$ is an odd function.
- (e) $\sup_{s_i} |sat(s_i)| \leq 1$.

The forms of the saturation function have been extensively studied. A piecewise linear (PWL) function is used in⁷ as the saturation function:

$$sat(s) = \begin{cases} -1 & s < -\delta \\ s/\delta & -\delta \leq s \leq \delta \\ 1 & s > \delta \end{cases}, \quad (10)$$

where δ is a positive constant. In quasi-SMC with the PWL function as the saturation function, the domain $[-\delta, \delta]$ is called the boundary layer. It can be concluded that the reaching velocity (\dot{S}) is a linear function of x . Therefore, the state variable cannot reach the equilibrium point in finite time, which means that the dynamics performance of this controller will be reduced as well.

The hyperbolic tangent function has also been chosen as a saturation function:

$$sat(s) = \tanh(ks), \quad (11)$$

where $k > 0$. An example of different saturation functions is shown in **FIGURE 2**.

The effect of parameter k was discussed in previous research by several simulations⁹. However, the parameter was chosen by experience; therefore, the performance index has not been optimized. It is necessary to achieve a balance between chattering reduction and dynamics performance optimization.

2.2 | Integral Reinforcement Learning

In this subsection, we formulate the IRL methods based on the CT input-affine system (1). IRL represents a class of algorithms that find the nearly optimal controller for CT systems by learning from online data. Define the performance index used in this paper as

$$J(x_t, u) = \int_t^{\infty} r(x_\tau, u_\tau) d\tau, \quad (12)$$

where $r(x, u) = Q(x) + u^T R u \in \mathbb{R}$ is the cost-to-go function with $Q(x) \geq 0$ and $R > 0, \forall x \in \mathcal{D}$. The goal of both optimal control and the IRL algorithm is to find the optimal policy μ^* that can minimize the function J along the trajectory of x .

The value function plays a central role in estimating the performance of a policy. In this paper, the value function V^μ of an initial state with policy (control law) $u = \mu(x)$ can be defined as

$$V^\mu(z) := J(z, \mu(z)), \quad (13)$$

where $z \in \mathcal{D}$ is the initial state value $x(0)$ of the system. The domain Ω in state space \mathcal{D} is called the admissible region if for all $z \in \Omega$, the policy $\mu(x)$ is able to stabilize system (1). $\mu(x)$ is called an admissible policy in Ω . With an admissible policy, $V^\mu(z) < \infty$ is satisfied, and $V^\mu(x)$ can be considered a Lyapunov function of (1) in domain Ω . From Bellman's principle of optimality¹⁰, the optimal policy $\mu^*(x)$ can be obtained as an equation denoted by the value function:

$$\mu^*(x) = \arg \min_{\mu} V^\mu(x), \quad (14)$$

where the value function of the optimal policy $V^{\mu^*}(x)$ is also the optimal value function that denotes the minimized performance index:

$$V^{\mu^*}(x) = V^*(x) = \min_{\mu} V^\mu(x). \quad (15)$$

Define the Hamiltonian as

$$H(x, u, \lambda) := r(x, u) + p^T (f + gu). \quad (16)$$

Take the multiplier as $p = \nabla V$. The Hamiltonian can be regarded as a CT version of the Q-function²¹, which is commonly used to denote the value of different actions in discrete-time RL algorithms.

An integral-temporal difference (I-TD) method to estimate the value function of policy $\mu(x)$ in a continuous-time model was proposed in¹⁸. The cost-to-go function can be written in interval form as:

$$V^\mu(x(t+T)) - V^\mu(x(t)) = - \int_t^{t+T} r(x(\tau), u(\tau)) d\tau, \quad (17)$$

where $[t, t+T]$ is a small-time interval and the value function can be obtained by solving the I-TD equation. This estimation is also called a policy evaluation in RL algorithms.

After the policy evaluation, the value function of the current policy is estimated. By solving the equation below, we find the maximum value of the Hamiltonian:

$$\frac{\partial H}{\partial u} = 2Ru + g^T (\nabla V^\mu) = 0, \quad (18)$$

and the greedy policy of this estimated value function is obtained as

$$\mu^{next} = -\frac{1}{2} R^{-1} g^T(x) \nabla V^\mu(x). \quad (19)$$

The solution to (19) is called the policy improvement in the DP and RL algorithms. By repeatedly performing policy evaluation and improvement, we can cause the value function and policy to converge to optimum if an initial admissible policy μ_0 is applied for the first iteration¹⁸. The iterative updating formulas are obtained as

$$\begin{cases} V_{i+1}(x(t+T)) - V_i(x(t)) = - \int_t^{t+T} r(x(\tau), \mu_i(\tau)) d\tau \\ \mu_{i+1} = -\frac{1}{2} R^{-1} g^T(x) \nabla V_i \end{cases}. \quad (20)$$

After the value function converges to the optimum $V^*(x)$, the optimal policy is obtained:

$$\mu^*(x) = -\frac{1}{2} R^{-1} g^T(x) \nabla V^*(x). \quad (21)$$

It is worth noting that the policy improvement step above requires *a priori* knowledge of the system drift dynamics $g(x)$. Integral Q-learning I, a model-free method that can perform both policy evaluation and policy improvement without knowledge of the system dynamics $f(x)$ or $g(x)$, was proposed in¹⁹. The exploration signal e is introduced to relax *a priori* knowledge requirement of the dynamics system:

$$\dot{x} = f(x) + g(x)(u + e), \quad (22)$$

where e is a nonzero exploration signal that satisfies the persistence of excitation (PE) condition²². Solve a single I-TD equation

$$\begin{aligned} & V_{i+1}(x(t+T)) - V_{i+1}(x(t)) \\ &= - \int_t^{t+T} [r(x, u) + 2\mu_{i+1}^T Re_\tau] d\tau, \end{aligned} \quad (23)$$

the value function estimation and updating policy are obtained at the same time. The system will not be stable at the origin with exploration, which enables the sensors to collect sufficient data online and perform policy improvement without explicitly using the information of $g(x)$. In other words, integral Q-learning I is a completely model-free IRL method with *a priori* knowledge requirement of the initial admissible policy only¹⁹.

The solution of (23) is approximated by collecting online data and minimizing the least-squares error. In these previous works, polynomial regression neural networks based on batch least squares (BLS) were the most commonly used method to perform the approximation.

3 | IRL-BASED CHATTERING REDUCTION METHOD

3.1 | Constrained Optimization Problem using IRL

In this section, we describe our work based on the two kinds of control algorithms mentioned above by combining model-based SMC and the model-free approximation of value function and learned policy. Split the general control law (7) into the following two parts:

$$\begin{cases} u_{p1} = -(C^T g)^{-1}(C^T f + W S) \\ u_{p2} = -(C^T g)^{-1} K \text{sat}(S) \end{cases}. \quad (24)$$

The signum function can be regarded as a discontinuous saturation function in u_{p2} .

For system (22), the main goal of the chattering reduction method presented in this paper is to find the saturation function that optimizes the performance index (12). To satisfy requirements (a)–(e) mentioned in section 2, we set these conditions as constraints of an optimization problem.

The objective function with these constraints is denoted as

$$\begin{aligned} & \min_{\text{sat}(S)} \int_t^\infty r(x_\tau, u_\tau) d\tau \\ & \text{s.t. } \text{sat}(s_i) \cdot \text{sgn}(s_i) > 0 \quad (s_i \neq 0), \\ & \lim_{s_i \rightarrow \infty} \text{sat}(s_i) = \text{sgn}(s_i), \\ & \text{sat}(s_i) = -\text{sat}(-s_i), \\ & \sup_{s_i} |\text{sat}(s_i)| \leq 1, \end{aligned} \quad (25)$$

where $u_\tau = u_{p1} + u_{p2}$.

In this paper we try to find a solution to (25) using an algorithm based on integral Q-learning I. First, we consider the unconstrained optimization problem described by u_{p1} and u_{p2} . By substituting the general control law (7) into the equation above,

Algorithm 1 IRL-Based Chattering Reduction**1. Initialization:**

Find an initial control policy $u_0 = u_{p1} + u_{p2,0}$ and let $i \leftarrow 0$.

2. Online data collection:

Apply the sliding mode control policy u_i and collect information for $\tau = 0 \rightarrow NT$ with an initial state $x(0) = z$.

3. Policy evaluation & improvement:

Solve (26).

4. Stopping criterion:

Let $i \leftarrow i + 1$. Update policy $u_{p2,i}$ and initialize the state $x \leftarrow z$ and time $t \leftarrow 0$.

Go to step 2, until

$$\sup_{x \in \mathcal{D}} \| \text{sat}_{i+1}(s_j) - \text{sat}_i(s_j) \| < \varepsilon, j = 1, 2, \dots, m \quad (27)$$

where ε is a small, positive constant.

we can obtain the optimization problem with no constraints as the iterative equation below:

$$\begin{aligned} V_{i+1}(x(t+T)) - V_{i+1}(x(t)) + \int_t^{t+T} 2u_{p2,i+1}^T R e_\tau d\tau \\ = - \int_t^{t+T} (Q(x) + u_i^T R u_i + 2u_{p1}^T R e_\tau) d\tau, \end{aligned} \quad (26)$$

where $u_{p2,0} = -(C^T g)^{-1} K \text{sgn}(S)$. During the iteration, the first part of the control law u_{p1} is not updated.

The IRL-based chattering reduction algorithm is shown in Algorithm 1. However, this IRL method is applied to solve the unconstrained optimal control problem. Thus, an IRL-based chattering reduction method is proposed in this paper to meet the needs of problem (25).

3.2 | Online Implementation Using an Approximation NN

To find the solution of (26) under constraints, the value function and the policy, which is denoted by the saturation function, can be parameterized as

$$\hat{V}(x) = \hat{\theta}_c^T \psi(x) \quad (28)$$

and

$$\text{sat}(S) = \tanh(S) + \Phi^T(S) \hat{\theta}_a \quad (29)$$

respectively, where

$$\begin{aligned} \tanh(S) &= [\tanh(s_1), \dots, \tanh(s_m)]^T, \\ \Phi(S) &= [\Phi^T(s_1), \dots, \Phi^T(s_m)]^T, \end{aligned}$$

and

$$\Phi(s_i) = [\phi_1(s_i), \phi_2(s_i), \dots, \phi_p(s_i)].$$

The value function $V(x)$ and the saturation function $\text{sat}(S)$ can be approximated by a critic NN and an actor NN, respectively. $\psi(x)$ and $\phi_j(s_i)$ ($j = 1, 2, \dots, p$) are nonlinear basis functions. $\hat{\theta}_a$ and $\hat{\theta}_c$ are the weight vectors. The hyperbolic tangent function $\tanh(s)$ used in⁹ can be regarded as a special case of function (29) when the dimension of the input vector $m = 1$ and $\hat{\theta}_a$ is a null vector.

In this paper, the quadratic polynomial basis function is used to approximate the value function, which can be obtained using the Kronecker product:

$$\begin{aligned} \psi(x) &= x \otimes x \\ &= [x_1^2, x_1 x_2, \dots, x_1 x_n, x_2 x_1, \dots, x_2 x_n, \dots, x_n^2]^T. \end{aligned}$$

To make $\text{sat}(s_i)$ symmetric about the origin $s_i = 0$ and satisfy the condition $\lim_{s_i \rightarrow \infty} \text{sat}(s_i) = \text{sgn}(s_i)$, the symmetry radial basis function (SRBF) is used in this paper:

$$\phi_j(s_i) = e^{-\gamma_j(s_i - r_j)^2} - e^{-\gamma_j(s_i + r_j)^2},$$

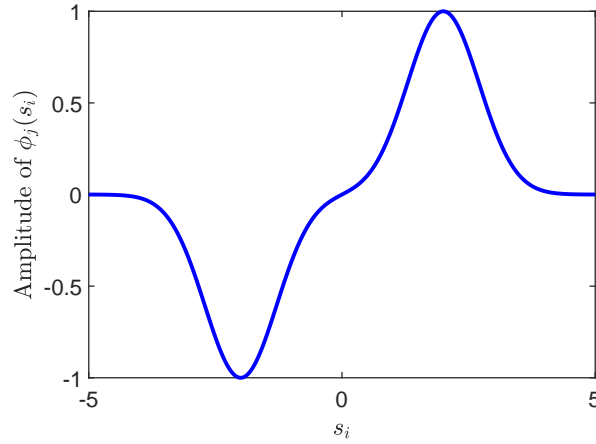


FIGURE 3 An example of the symmetric radial basis function where $\gamma_j = 1$ and $r_j = 2$.

where γ_j and r_j are both positive constants.

A single RBF neuron has the local response property: it can generate high-level gain only if the input is close to its center. As shown in **FIGURE 3**, the symmetry RBF will generate the maximum (or minimum) output if the input $s_i = r_j$ (or $-r_j$). It is proved that the RBF network has the best ability to fit locally continuous nonlinear functions²³. Therefore, the RBFNN may achieve satisfactory effects in approximating the saturation function within a boundary layer.

The iterative equation is presented as:

$$\begin{aligned}
 & \hat{\theta}_{c,i+1}^T (\psi(x(t+T)) - \psi(x(t))) \\
 & + 2\hat{\theta}_{a,i+1}^T \int_t^{t+T} \Phi(S)G^T e_\tau d\tau \\
 & = - \int_t^{t+T} 2e_\tau^T G \tanh(S) + (Q(x) + u_i^T R u_i + 2u_{p1}^T R e_\tau) d\tau
 \end{aligned} \tag{30}$$

where $G = R(C^T g)^{-1}K$. After N periods of data are collected, the N -dimensional linear equations can be obtained as

$$\Psi_i \hat{\Theta}_{i+1} = \Xi_i, \tag{31}$$

where:

$$\begin{aligned}
 & \hat{\Theta}_{i+1} = [\hat{\theta}_{c,i+1}, \hat{\theta}_{a,i+1}]^T, \\
 & \Psi_i = \begin{bmatrix} \psi^T(x)|_t^{t+T} & 2 \int_t^{t+T} e_\tau^T G \Phi^T(S) d\tau \\ \psi^T(x)|_{t+T}^{t+2T} & 2 \int_{t+T}^{t+2T} e_\tau^T G \Phi^T(S) d\tau \\ \vdots & \vdots \\ \psi^T(x)|_{t+(N-1)T}^{t+NT} & 2 \int_{t+(N-1)T}^{t+NT} e_\tau^T G \Phi^T(S) d\tau \end{bmatrix}, \\
 & \Xi_i = [\xi_1, \xi_2, \dots, \xi_N]^T
 \end{aligned}$$

and the elements of vector Ξ_i can be obtained as:

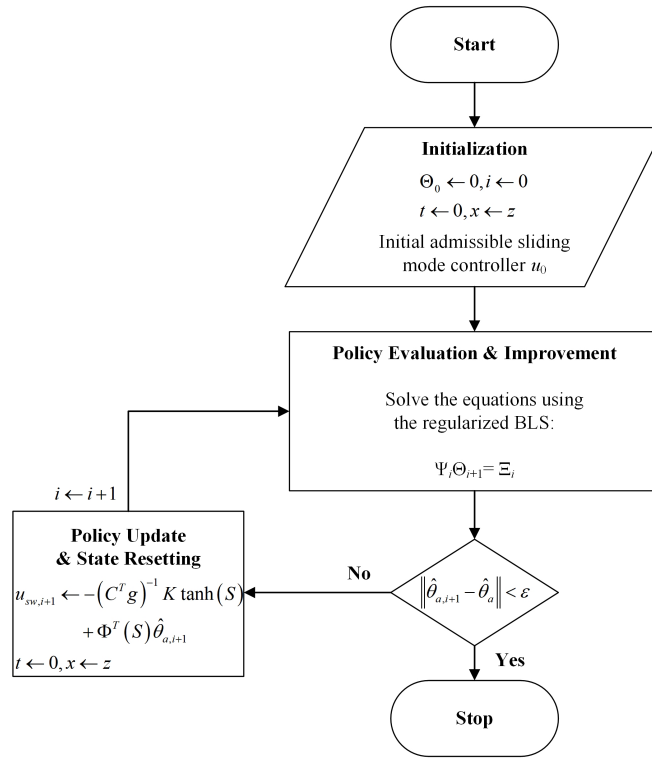


FIGURE 4 The flowchart of Algorithm 1 using an approximation NN.

$$\begin{aligned} \xi_j = & -2 \int_{t+(j-1)T}^{t+jT} e^{\tau T} G \tanh(S) \\ & - \int_{t+(j-1)T}^{t+jT} (Q(x) + u_i^T R u_i + 2u_{p1}^T R e_\tau) d\tau, \end{aligned}$$

where $j = 1, 2, \dots, N$.

Constraint conditions (a)–(d) in optimization problem (25) can be satisfied by using the RBFNN. The least-squares solution that minimizes the approximation error can be obtained as follows using the BLS algorithm:

$$\hat{\Theta}_{i+1} = (\Psi_i^T \Psi_i)^{-1} \Psi_i^T \Xi_i, \quad (32)$$

where $\Psi_i^\dagger = (\Psi_i^T \Psi_i)^{-1} \Psi_i^T$ is the Moore-Penrose pseudoinverse matrix of Ψ_i . **FIGURE 4** shows the flowchart of our Algorithm 1 using the approximation NN.

The number of sample periods N must be sufficient such that the following assumption is satisfied.

Assumption 1. The rank of matrix Φ_i meets the following condition:

$$\text{rank}(\Phi_i) \geq L_{\hat{\Theta}}, \quad (33)$$

where $L_{\hat{\Theta}}$ is the number of elements in vector $\hat{\Theta}$.

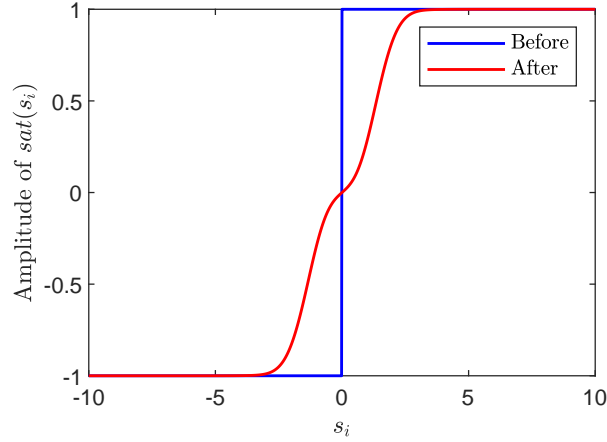


FIGURE 5 Example 1: Saturation function learned by the approximation NN using the regularization method. The weight vector in this simulation is iterated 10 times.

The ordinary BLS algorithm, however, cannot satisfy condition (e). In this paper, constraint (e) is modified as a penalty function and the objective function can be rewritten as

$$\min_{sat(S)} \int_0^{\infty} r(x, u) d\tau + \lambda \|\hat{\Theta}\|_2^2 \quad (34)$$

$$s.t. \quad sat(S) = \tanh(S) + \Phi^T(S)\hat{\theta}_a,$$

where $\lambda > 0$ is called the penalty term. Similar to (32), the weight updating formula using the penalty function method is

$$\hat{\Theta}_{i+1} = (\Psi_i^T \Psi_i + \lambda I)^{-1} \Psi_i^T \Xi_i. \quad (35)$$

The update rule above is called the ℓ_2 -regularization LS algorithm. The regularization method is also an effective way to improve the performance of the approximator by avoiding overfitting in regression tasks²⁴. The result of using the regularization method is shown in the next section. The approximation can also be accomplished by the recursive least squares (RLS) algorithm, which can perform the policy evaluation step at each time interval T .

4 | NUMERICAL SIMULATION

In this section, the chattering reduction method proposed in this paper is simulated with two examples to verify its effectiveness.

4.1 | Example 1: Simple Single-input Single-output (SISO) System

Consider an SISO linear system

$$\dot{x} = Ax + Bu, \quad (36)$$

where

$$A = \begin{bmatrix} 0 & 1 \\ 0 & -25 \end{bmatrix}, B = \begin{bmatrix} 0 \\ 133 \end{bmatrix}$$

and the cost function is defined as

$$r(x, u) = 10x_1^2 + 10x_2^2 + u^2.$$

The sliding mode function can be obtained as $S = C^T x$ where $C = [15, 1]^T$. The other parameters in the sliding mode controller are as follows: $W = 10$ and $K = 10$, and the initial control policy is

$$\begin{cases} u_{p1} = -(C^T B)^{-1}(C^T Ax + WS) \\ u_{p2,0} = -(C^T B)^{-1}K \operatorname{sgn}(S) \end{cases}. \quad (37)$$

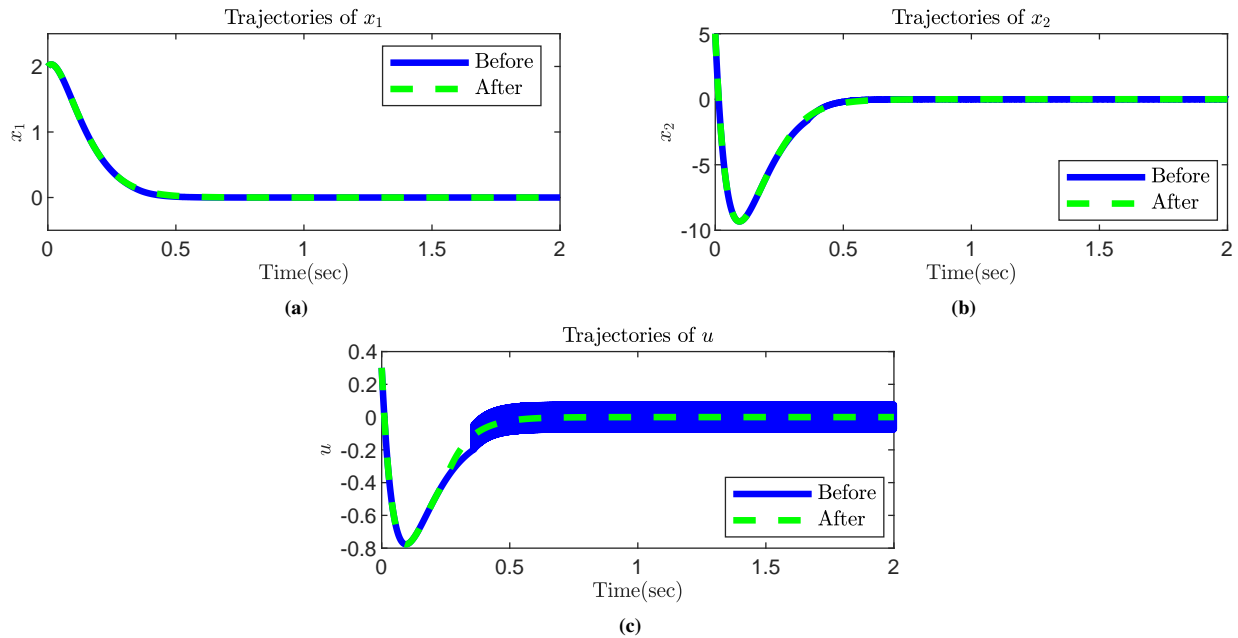


FIGURE 6 Example 1: Trajectories of the state variables (a) x_1 , (b) x_2 and input (c) u . Blue solid lines indicate the trajectories before using the chattering reduction algorithm, and the green dotted lines indicate the trajectories after learning.

In this example, the value function can be approximated by a linear combination of quadratic polynomials. We choose the basis of the critic NN as

$$\psi(x) = [x_1^2, x_1x_2, x_2x_1, x_2^2]^T.$$

The actor NN is initialized as a single-layer network with 7 symmetry RBF neurons. The hyperparameters γ_j of the SRBFs are all chosen as $\gamma_j = 1$. The width of the boundary layer should be sufficiently small. Thus, the centers of these neurons we choose in this example are near the origin and can be described as a vector

$$\begin{aligned} \text{vec}(r_j) &= [r_1, r_2, \dots, r_7]^T \\ &= [0.01, 0.03, 0.05, 0.1, 0.2, 0.5, 1]^T. \end{aligned}$$

Here, the number of sampling periods per iteration $N = 200$, and the time interval $T = 0.01$ s. The system starts at an initial state $z = [2, 5]^T$. The learning controller performs the policy evaluation and improvement every 2 seconds, and the states are reset to z before the next iteration. During the iteration, the exploration signal is set as $e = 0.1 \sin(\tau)$, and the regularization (penalty) term $\lambda = 0.01$.

The saturation function learned by the NN after 10 iterations is shown in **FIGURE 5**. The weight vector converges to

$$\begin{aligned} \hat{\theta}_a &= [-0.0050, -0.0150, -0.0250, -0.0498, \\ &\quad -0.0981, -0.2203, -0.2933]^T. \end{aligned}$$

The result shows the effectiveness of the presented algorithm in both decreasing the performance index along the trajectories and avoiding chattering near the switching manifold. When an ℓ_2 regularization term is added to (32), the regularized BLS method (35) minimizes the weighted sum of the approximation error and ℓ_2 -norm of the weight vector $\hat{\Theta}$. **FIGURE 8** shows the effect of our method in decreasing the performance index. The blue line denotes the total cost of our controller with exploration during the iteration. In this example, we choose the baseline to be the saturation function $\text{sat}(s_i) = \tanh(s_i)$, which is presented in⁹, to show the effectiveness of our method. This figure shows that the total cost of the system in each episode monotonically decreases to convergence.

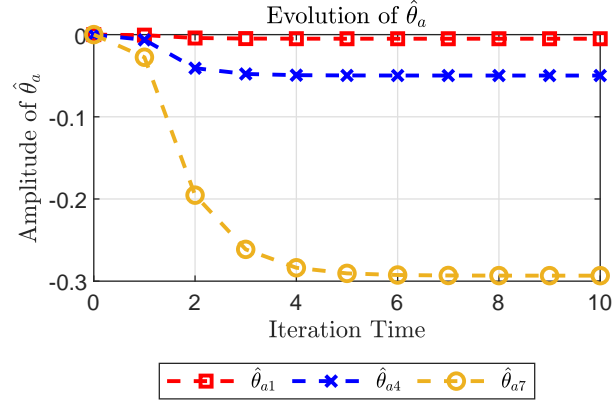


FIGURE 7 Example 1: Evolution of the weights $\hat{\theta}_{a1}$, $\hat{\theta}_{a4}$ and $\hat{\theta}_{a7}$ after 10 learning episodes.

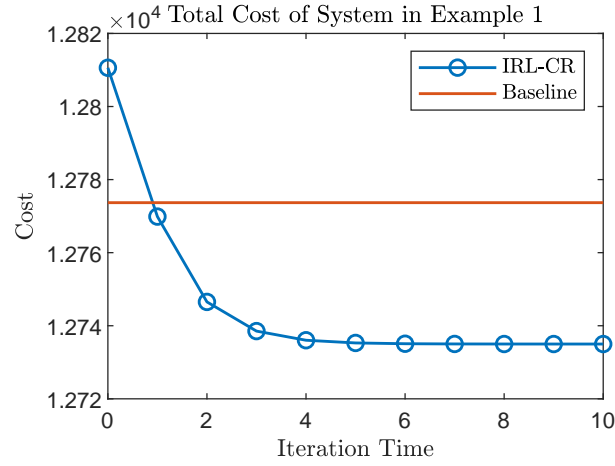


FIGURE 8 Example 1: The total cost of the system in each episode.

4.2 | Example 2: Application to a Two-wheeled Variable Structure Robot (VSR)

Consider an application to the dynamics model of our previous work, i.e., a two-wheeled VSR²⁵. It is a wheeled robot that can switch its structure between Segway mode, which can be regarded as an inverted pendulum, and self-driving bicycle mode. In this paper we focus on the learning progress of a VSR working in Segway mode, which is designed for the robot to autonomously drive under flat and broad road conditions.

FIGURE 9 shows the diagram of the VSR model. The task in this example is to stabilize the robot without considering the motion path and the final position. The dynamics model of the VSR in Segway mode is obtained as

$$\begin{cases} \dot{x}_1 = x_2 \\ \dot{x}_2 = 145.1697 \sin x_1 - 1.1790 u_1 - 1.1790 u_2 \\ \dot{x}_3 = -36.2317 \sin x_1 + 0.7819 u_1 + 0.7819 u_2, \\ \dot{x}_4 = -55.5691 \sin x_1 + 4.3571 u_1 - 0.2575 u_2 \\ \dot{x}_5 = -55.5691 \sin x_1 - 0.2575 u_1 + 4.3571 u_2 \end{cases} \quad (38)$$

where x_1 is the pitch angle of the robot and x_2 is the angular velocity of x_1 . x_3 is the angular velocity of the yaw angle. x_4 and x_5 are the angular velocity of the left- and right-wheel steering angles, respectively. To stabilize the state vector $x =$

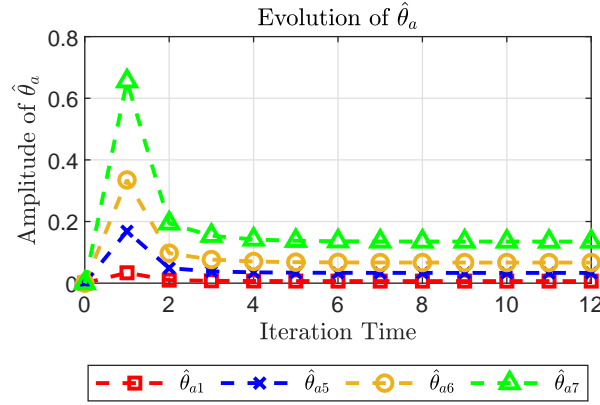


FIGURE 11 Example 2: Evolution of the weights $\hat{\theta}_{a1}$, $\hat{\theta}_{a5}$, $\hat{\theta}_{a6}$ and $\hat{\theta}_{a7}$ after 12 learning episodes.

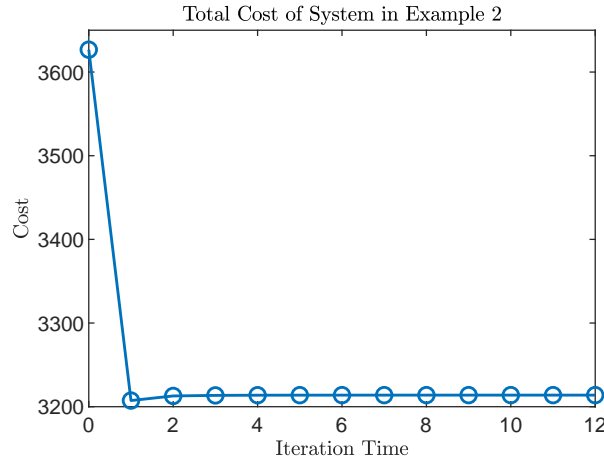


FIGURE 12 Example 2: The total cost of the system in each episode.

the weight vector converged to

$$\hat{\theta}_a = [0.0067, 0.0133, 0.0200, 0.0267, \\ 0.0333, 0.0668, 0.1350, 0.2057]^T.$$

The initial state was set as $z = [0.1, 0, 0, 0, 0]^T$ in this simulation. Similar to example 1, a data plot of the total cost is shown in **FIGURE 12**. The cost reached its minimum after the first iteration. The weight vector $\hat{\Theta}$, however, was too large to satisfy condition (e) and was punished by the regularization term.

To easily show the system response, we set the unit of x_1 in **FIGURE 13** (a) as degrees instead of radians, while the unit of the angular velocity was set as rad/s in the corresponding figure. As shown in **FIGURE 13**, the trajectories of the state variables nearly identical in the simulations before and after learning. The chattering phenomenon of the input variables u_1 and u_2 disappeared after using the saturation function learned from the sampling data.

Remark 1. In sections 2 and 4, we compared our method with different quasi-SMC methods. The saturation function learned by our algorithm consists of the hyperbolic tangent function and several SRBFs. In theory, due to the differentiability and nonlinearity, our method can achieve better dynamics performance than the PWL function⁷. In section 4, we also showed the advantage of our method by comparing it with the baseline⁹ in a simulation.

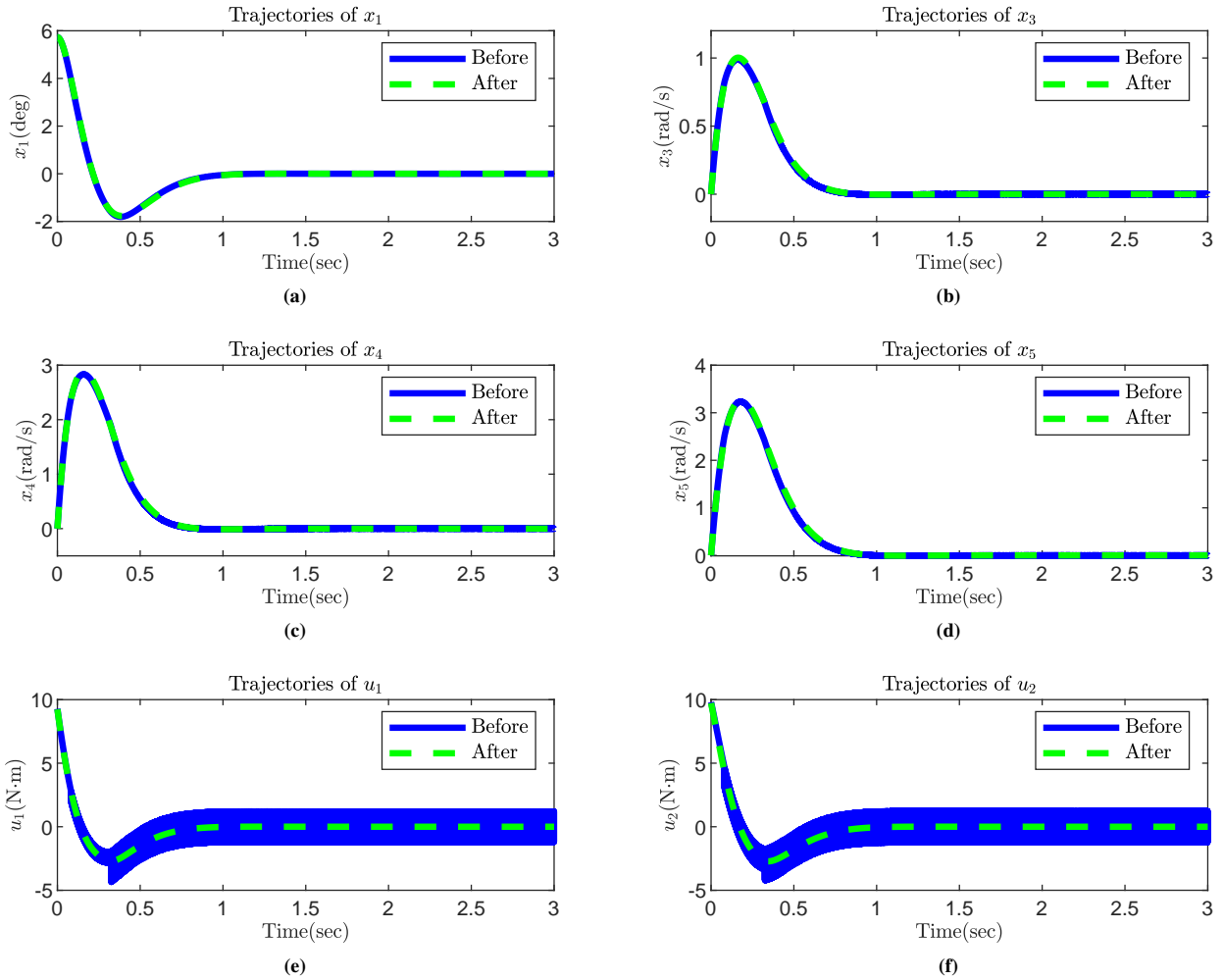


FIGURE 13 Example 2: Trajectories of the state variables (a) x_1 , (b) x_3 , (c) x_4 , and (d) x_5 and the input (e) u_1 and (f) u_2 .

Remark 2. As mentioned above, the quasi-SMC using the hyperbolic tangent function⁹ is a special case of our method with the weight vector of the actor NN set as 0. Thus, the iteration can also start with it instead of the traditional SMC. The simulation with two examples shows that our method can converge to the minimum value of the performance index under the condition of satisfying the constraints we set in this paper. Due to the training period of NNs, the algorithm requires a sufficient computing capability of the processor to ensure real-time computation online if the controlled object has a high-dimensional state and input space.

Remark 3. Our algorithm is based on the integral Q-learning I¹⁹, which is an online policy iteration method. An initial admissible controller is needed in this method to ensure the stability of the system. To satisfy the requirement, we set the initial controller as a model-based sliding mode controller. Thus, the algorithm proposed in this paper can be regarded as a combination of pure model-based and model-free methods. The sliding mode controller designed offline can avoid numerous inefficient, meaningless exploration actions during the learning period, while the model-free method can help the controller optimize the performance index.

5 | CONCLUSIONS

The dilemma of reducing chattering and maintaining dynamics performance was discussed in this paper, and a chattering reduction method based on IRL using an approximation NN was proposed. The major advantage of this new method is that it can

reach a balance between improving the performance index and reducing chattering. In section 4, two simulation examples, especially the second one, verified the effectiveness of the proposed algorithm, and showed its potential in real-world applications, e.g., as a stable, self-learning controller of robots. The combination of our work in this paper and high-order SMC is a valuable research direction for the future. The robustness improvement of the proposed controller is also worth studying.



APPENDIX

Dynamics Modeling of the VSR in Segway mode

.1 Notations & Kinematic Analysis

In this paper, we define four different coordinate systems, which are also shown in **FIGURE 9**, to describe the motions of the robot:

$e^{(0)}$ denotes the coordinate system fixed on the ground. Axis $e_1^{(0)}$ is vertical outward, $e_2^{(0)}$ is horizontal to the right and $e_3^{(0)}$ is vertical up to the ground.

$e^{(1)}$ denotes the coordinate system relative to the center of mass (CoM) of the bicycle frame.

$e^{(2)}$ denotes the coordinate system relative to the CoM of the left wheel and the wheel rolls along the direction of $e_1^{(2)}$.

$e^{(3)}$ denotes the coordinate system relative to the CoM of the right wheel and the wheel rolls along the direction of $e_1^{(3)}$.

The physical parameters and notations of the states and inputs of the model are shown in **TABLE 1** and **2**.

The angular velocities of the bicycle frame, left fork and right fork are denoted as ω_1 , ω_2 , and ω_3 , respectively. In coordinate system $e^{(0)}$, both of these parameters have the same value:

$$\omega_1 = \omega_2 = \omega_3 = (0, -\dot{q}_1, -\dot{q}_2)^T. \quad (1)$$

In Segway mode, the coordinate systems $e^{(1)}$, $e^{(2)}$, and $e^{(3)}$ are parallel to each other. The transformation matrices of coordinates from $e^{(1)}$ to $e^{(2)}$ and $e^{(3)}$ are both three-dimensional unit matrix. Thus, the angular velocity of the left wheel in $e^{(2)}$ and the angular velocity of the right wheel in $e^{(3)}$ are obtained as

$$\omega_4 = \omega_2 + (0, -\dot{q}_3, 0)^T = (0, -\dot{q}_1 - \dot{q}_3, -\dot{q}_2)^T, \quad (2)$$

and

$$\omega_5 = \omega_3 + (0, -\dot{q}_4, 0)^T = (0, -\dot{q}_1 - \dot{q}_4, -\dot{q}_2)^T, \quad (3)$$

respectively.

It is assumed that both wheels perform a pure rolling motion on the ground. Thus, the velocity of the CoM of the left wheel in $e^{(2)}$ is

$$v_4 = -\omega_4 \times (0, 0, r)^T = (r\dot{q}_1 + r\dot{q}_3, 0, 0)^T. \quad (4)$$

Similarly, the velocity of the CoM of the right wheel in $e^{(3)}$ is

$$v_5 = -\omega_5 \times (0, 0, r)^T = (r\dot{q}_1 + r\dot{q}_4, 0, 0)^T. \quad (5)$$

The velocity of other components in coordinate system $e^{(1)}$ can be converted from v_4 and v_5 . The velocity of the left fork and the right fork can be obtained as

$$v_2 = v_4 + \omega_2 \times (0, 0, -h)^T = ((h+r)\dot{q}_1 + r\dot{q}_3, 0, 0)^T \quad (6)$$

and

$$v_3 = v_5 + \omega_3 \times (0, 0, -h)^T = ((h+r)\dot{q}_1 + r\dot{q}_4, 0, 0)^T, \quad (7)$$

respectively. The velocity of the frame is

$$\begin{aligned} v_1 &= \frac{1}{2}(v_4 + v_5) + \omega_1 \times (0, -l, -2h)^T \\ &= ((2h+r)\dot{q}_1 + l\dot{q}_2 + \frac{1}{2}r(\dot{q}_3 + \dot{q}_4), 0, 0)^T. \end{aligned} \quad (8)$$

TABLE 1 State Variables and Inputs of the VSR

Notation	Meaning
q_1	Pitch angle of the VSR.
q_2	Yaw angle of the VSR.
q_3	Roll angle of the left wheel.
q_4	Roll angle of the right wheel.
τ_3	Torque the controller applies to the left wheel.
τ_4	Torque the controller applies to the right wheel.

TABLE 2 Physical Parameters of the VSR

Notation	Meaning	Value
J_{1x}	The moment of inertia (MoI) of the bicycle frame about the axis $e_1^{(1)}$.	1.18 kg·m ²
J_{1y}	The MoI of the bicycle frame about the axis $e_2^{(1)}$.	0.06 kg·m ²
J_{1z}	The MoI of the bicycle frame about the axis $e_3^{(1)}$.	1.21 kg·m ²
J_{2x}	The MoI of the bicycle fork about the axis $e_1^{(1)}$.	0.014 kg·m ²
J_{2y}	The MoI of the bicycle fork about the axis $e_2^{(1)}$.	0.017 kg·m ²
J_{2z}	The MoI of the bicycle fork about the axis $e_3^{(1)}$.	0.0046 kg·m ²
J_{3x}	The MoI of the wheel about the axis $e_1^{(2)}$ or $e_1^{(3)}$.	0.03 kg·m ²
J_{3y}	The MoI of the wheel about the axis $e_2^{(2)}$ or $e_2^{(3)}$.	0.05 kg·m ²
J_{3z}	The MoI of the wheel about the axis $e_3^{(2)}$ or $e_3^{(3)}$.	0.02 kg·m ²
r	The wheel radius.	0.17 m
$2h$	The height difference between the CoM of a wheel and the CoM of the bicycle frame.	0.36 m
$2l$	The distance between the CoMs of both wheels.	0.68 m
m_1	The mass of the bicycle frame.	23.14 kg
m_2	The mass of a bicycle fork.	0.5 kg
m_3	The mass of a wheel.	3.8 kg

.2 Dynamics Analysis Using Chaplygin's Equation

Chaplygin's equation is a useful tool for performing a dynamics modeling, which is denoted as

$$\begin{aligned}
 & \frac{d}{dt} \frac{\partial \tilde{T}}{\partial \dot{q}_\sigma} - \frac{\partial \tilde{T}}{\partial q_\sigma} - \frac{\partial U}{\partial q_\sigma} \\
 & + \sum_{\beta=1}^{\eta} \frac{\partial T}{\partial \dot{q}_{\zeta+\beta}} \sum_{\gamma=1}^{\zeta} \left(\frac{\partial B_{\zeta+\beta,\gamma}}{\partial q_\sigma} - \frac{\partial B_{\zeta+\beta,\sigma}}{\partial q_\gamma} \right) \dot{q}_\gamma, \\
 & = \tilde{Q}_\sigma (\sigma = 1, 2, \dots, \zeta)
 \end{aligned} \tag{9}$$

where ζ is the number of holonomic constraints, with $\zeta = 4$ in Segway mode. η denotes the number of nonholonomic constraints of the system and $\eta = 2$ in this model. \tilde{T} or T denotes the total kinetic energy with or without the nonholonomic constraints and U is the total potential energy of the system. q_σ and \tilde{Q}_σ are generalized independent coordinates and their corresponding generalized moments of force. In nonholonomic constraint form $\dot{q}_{\zeta+\beta}$, the coefficient of \dot{q}_γ is denoted as $B_{\zeta+\beta,\gamma}$.

The nonholonomic constraint of the left wheel along $e_1^{(2)}$ and the right wheel along $e_1^{(3)}$ is obtained as

$$\dot{q}_5 = r\dot{q}_1 + r\dot{q}_3 \tag{10}$$

and

$$\dot{q}_6 = r\dot{q}_1 + r\dot{q}_4, \tag{11}$$

respectively, due to the pure rolling motion assumption. The total kinetic energy, including the rotation and translation kinetic energy, is denoted as

$$T = \sum_{i=1}^5 (T_{1i} + T_{2i}) \quad (i = 1, 2, 3, 4, 5), \quad (12)$$

where the rotation kinetic energy is

$$T_{1i} = \frac{1}{2} J_i \omega^T \omega = \frac{1}{2} (J_{ix} \omega_{ix}^2 + J_{iy} \omega_{iy}^2 + J_{iz} \omega_{iz}^2). \quad (13)$$

The translation kinetic energy of each component with the nonholonomic constraints is obtained as

$$\begin{cases} T_{21} = \frac{1}{2} m_1 v_1^T v_1 \\ T_{22} = \frac{1}{2} m_2 v_2^T v_2 \\ T_{23} = \frac{1}{2} m_2 v_3^T v_3 \\ T_{24} = \frac{1}{2} m_3 (\dot{q}_5^2 + v_{4z}^2) \\ T_{25} = \frac{1}{2} m_3 (\dot{q}_6^2 + v_{5z}^2) \end{cases}. \quad (14)$$

The translation kinetic energy of the left and right wheels without nonholonomic constraints can be denoted as

$$\tilde{T}_{24} = \frac{1}{2} m_3 v_4^T v_4 \quad (15)$$

and

$$\tilde{T}_{25} = \frac{1}{2} m_3 v_5^T v_5, \quad (16)$$

respectively. Substituting (12)–(16) into (9), the Chaplygin dynamics equations can be obtained as (17)–(20):

$$\begin{aligned} 0 = & -2gh(m_1 + m_2) \sin q_1 + (m_1 + 2m_2 + 2m_3)r^2 \ddot{q}_1 \\ & + (J_{1y} + 2(J_{2y} + J_{3y} + h^2(2m_1 + m_2)r + lm_1(2h + r))\ddot{q}_2 \\ & + \frac{1}{2}(2J_{3y} + 2h(m_1 + m_2)r + (m_1 + 2m_2 + 2m_3)r^2)\ddot{q}_3 \\ & + \frac{1}{2}(2J_{3y} + 2h(m_1 + m_2)r + (m_1 + 2m_2 + 2m_3)r^2)\ddot{q}_4 \end{aligned} \quad (17)$$

$$\begin{aligned} 0 = & lm_1(2h + r)\ddot{q}_1 + (J_{1z} + 2J_{2z} + 2J_{3z} + l^2 m_1)\ddot{q}_2 \\ & + \frac{1}{2}lm_1 r \ddot{q}_3 + \frac{1}{2}lm_1 r \ddot{q}_4 \end{aligned}, \quad (18)$$

$$\begin{aligned} \tau_3 = & \frac{1}{2}(2J_{3y} + r(2h(m_1 + m_2) + (m_1 + 2m_2 + 2m_3)r))\ddot{q}_1 \\ & + \frac{1}{2}lm_1 r \ddot{q}_2 + (J_{3y} + (\frac{1}{4}m_1 + (m_2 + m_3))r^2)\ddot{q}_3 + \frac{1}{4}m_1 r^2 \ddot{q}_4 \end{aligned}, \quad (19)$$

$$\begin{aligned} \tau_4 = & \frac{1}{2}(2J_{3y} + r(2h(m_1 + m_2) + (m_1 + 2m_2 + 2m_3)r))\ddot{q}_1 \\ & + \frac{1}{2}lm_1 r \ddot{q}_2 + (J_{3y} + (\frac{1}{4}m_1 + (m_2 + m_3))r^2)\ddot{q}_4 + \frac{1}{4}m_1 r^2 \ddot{q}_3 \end{aligned}. \quad (20)$$

By substituting the values of the parameters and performing identical deformations, we can obtain the dynamics model of the VSR (38).

References

1. Utkin V. Variable structure systems with sliding modes. *IEEE Transactions on Automatic Control* 1977; 22(2): 212-222. doi: 10.1109/TAC.1977.1101446
2. Gao W, Hung J. Variable structure control of nonlinear systems: a new approach. *IEEE Transactions on Industrial Electronics* 1993; 40(1): 45-55.

3. Jiang K, Zhang J, Chen Z. A new approach for the sliding mode control based on fuzzy reaching law. *Proc. World Congr. Intelligent Control Autom. (WCICA)* 2002; 1: 656-660.
4. Ma D, Lin H. Chattering-free nonsingular fast terminal sliding-mode control for Permanent Magnet Synchronous Motor servo system. *Chinese Control Conf. (CCC)* 2016: 3463-3467.
5. Changbo X, Shaozhong C. Robust Finite-time Terminal Sliding Mode Control for a Class of Nonlinear Uncertain Systems. *Proc. IEEE Int. Conf. Autom., Electron. Electr. Eng. (AUTEEE)* 2019: 649-654.
6. Cui X, Zhao X, Guo Y, Li X, Hou P. Adaptive Fuzzy Terminal Sliding Mode Synchronization of Uncertain Newton-Leipnik Chaotic System. *Int. Conf. Control, Autom. Robot. (ICCAR)* 2020: 309-313.
7. Slotine J, Sastry S. Tracking control of non-linear systems using sliding surfaces with application to robot manipulators. *Int. J. Control* 1983; 38(2): 465-492.
8. Hung J, Nelms R. Using a boundary layer technique to reduce chatter in sliding mode controllers. *Conf. Proc. IEEE Appl. Power Electron. Conf. Expo. (APEC)* 1991: 195-201.
9. Monteiro J, Oliveira C, Aguiar M. Sliding mode control of brushless DC motor speed with chattering reduction. *IEEE Int. Symp. Ind. Electron. (ISIE)* 2015: 542-547.
10. Bellman R. *Dynamic Programming*. Princeton Univ. Press . 1957.
11. Sutton R, Barto A. *Reinforcement Learning: An Introduction*. Cambridge Univ. Press . 1998.
12. Werbos P. Using ADP to understand and replicate brain intelligence: the next level design. *Proc. IEEE Symp. Approx. Dyn. Program. Reinf. Learn. (ADPRL)* 2007: 209-216.
13. Mnih V, Kavukcuoglu K, Silver D, et al. Human-level control through deep reinforcement learning. *Nature* 2015; 518: 529-533.
14. Lillicrap T, Hunt J, Pritzel A, et al. Continuous control with deep reinforcement learning. *Int. Conf. Learn. Represent. (ICLR) - Conf. Track Proc.* 2016.
15. Silver D, Huang A, Maddison CJ, et al. Mastering the game of Go with deep neural networks and tree search. *Nature* 2016; 529: 484-489.
16. Hwangbo J, Lee J, Dosovitskiy A, et al. Learning agile and dynamic motor skills for legged robots. *Sci. Robotics* 2019; 4(26).
17. Kiumarsi B, Vamvoudakis KG, Modares H, Lewis FL. Optimal and autonomous control using reinforcement learning: a survey. *IEEE Transactions on Neural Networks and Learning Systems* 2018; 29(6): 2042-2062. doi: 10.1109/TNNLS.2017.2773458
18. Vrabie D, Lewis F. Neural network approach to continuous-time direct adaptive optimal control for partially unknown nonlinear systems. *Neural Netw.* 2009; 22(3): 237-246.
19. Lee J, Park J, Choi Y. Integral reinforcement learning for continuous-time input-affine nonlinear systems with simultaneous invariant explorations. *IEEE Transactions on Neural Networks and Learning Systems* 2015; 26(5): 916-932.
20. Hung J, Gao W, Hung J. Variable structure control: a survey. *IEEE Transactions on Industrial Electronics* 1993; 40(1): 2-22.
21. Mehta P, Meyn S. Q-learning and pontryagin's minimum principle. *Proc. IEEE Conf. Decis. Control (CDC) held jointly with Chinese Control Conf. (CCC)* 2009: 3598-3605. doi: 10.1109/CDC.2009.5399753
22. Green M, Moore J. Persistence of excitation in linear systems. *Syst. Control Lett.* 1986; 7(5): 351 - 360. doi: [https://doi.org/10.1016/0167-6911\(86\)90052-6](https://doi.org/10.1016/0167-6911(86)90052-6)
23. Girosi F, Poggio T. Networks and the best approximation property. *Biol. Cybern.* 1989; 63: 169-176.

24. Kolter J, Ng A. Regularization and feature selection in least-squares temporal difference learning. *Proc. Int. Conf. Mach. Learn. (ICML) 2009*: 521–528.
25. Guo L, Wu H, Song Y. Dynamic modeling of a variable structure two-wheeled robot during the mode switching process between segway mode and bicycle mode. *Chinese Intelligent Syst. Conf.(CISC) 2019*; 529: 671-681.